Hindawi
International Journal of Antennas and Propagation
Volume 2018, Article ID 7684742, 11 pages
https://doi.org/10.1155/2018/7684742

Research Article

Dual-Frequency Circularly Polarized Truncated Square Aperture Patch Antenna with Slant Strip and L-Shaped Slot for WLAN Applications

Sorana Niyamanon, Rewat Senathong, and Chuwong Phongcharoenpanich

Faculty of Engineering, King Mongkut's Institute of Technology Ladkrabang, Bangkok 10520, Thailand

Correspondence should be addressed to Chuwong Phongcharoenpanich; pchuwong@gmail.com

Received 1 March 2018; Revised 31 May 2018; Accepted 4 June 2018; Published 16 July 2018

Academic Editor: N. Nasimuddin

This research proposes a dual-frequency circularly polarized truncated square aperture patch antenna with slant stripline and L-shaped slot for WLAN applications. In the antenna design, the parameters were optimized and the WLAN-enabled dual-frequency (2.4 and 5.8 GHz) antenna was realized. Simulations were subsequently carried out for the impedance bandwidth ($|S_{11}|$) < −10 dB, axial ratio (AR) ≤ 3 dB, optimal gain, and bidirectional radiation pattern. To validate, an antenna prototype was fabricated and the experiments were undertaken. The simulated and experimental results are in good agreement. In essence, the proposed WLAN-enabled dual-frequency circularly polarized antenna is most suited for applications in the vertically and horizontally elongated areas, including in the tunnel, train carriage, and buildings.

1. Introduction

Recent decades have witnessed exponential growth in the utilization of circularly polarized (CP) antennas in wireless communications. The wider adoption of CP technology is attributable to alignment variability (i.e., horizontal, vertical, and diagonal) of the receiving antenna with reliable performance [1]. Previous research has experimented with diverse antenna structures to produce circular polarization (CP) [2–21].

One of the most important characteristic of the antenna is the bandwidth. There are various techniques developed solely for the bandwidth enhancement. The printed wide-slot antenna fed by a microstrip line [2] achieves a wide impedance bandwidth with a very simple structure consisting of a feeding strip and a square slot on the opposite site of an FR4 substrate. The bandwidth of wide-slot antenna can still be enhanced by introducing defected ground structure [3], using fractal-shaped slot [4].

Another important characteristic of the antenna is the polarization. Since mobile device used in the wireless communication system such as W-LAN application does not have a static placement, circularly polarized antenna is implemented in order to ensure that the receiver will always be able to pick up transmitted signal regardless of its positioning. The circular polarization characteristic of the antenna can be created by using two feeding ports with a difference in phase of 90 degrees [5]. However, the complexity of two feeding ports can be adjusted into one feeding port with an unequally split feeding structure [6, 7], modifying the feeding structure into an S-shape [8], or using sequential rotation feeding structure [9] instead. Nevertheless, instead of changing the feeding structure of the antenna, there are many different methods that could also result in the antenna being circularly polarized such as the modification of the slot structure using various shape slits [10], adding a pair of inverted L [11], implementing truncated corners [12], introducing a parasitic patch [13, 14], placing a parasitic unequal linear slots [15], T-shaped slot [16], or S-shaped slot [17], using two-diode controlled slot [18], and changing the main slot structure into a set of small square slots with multiple rectangular arms [19].

Nevertheless, W-LAN application operated on two frequency bands. Thus, the antenna must also have a dual-band characteristic. The stacked antenna [20] uses two circularly polarized antennas of the different frequency

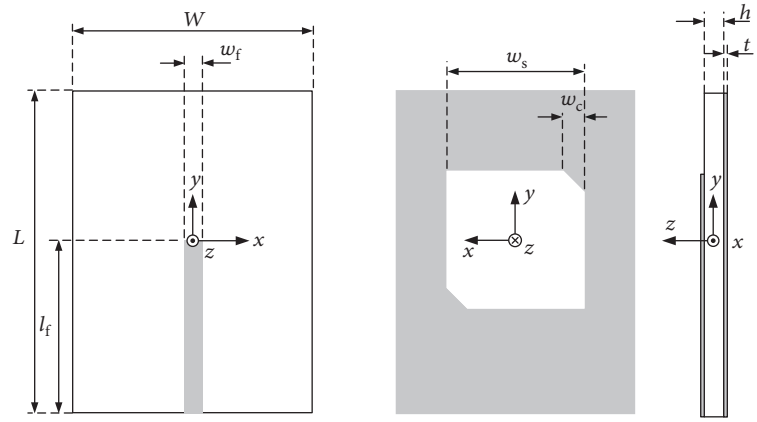

Figure 1: Initial design of the truncated square patch antenna (front view, rear view, and side view).

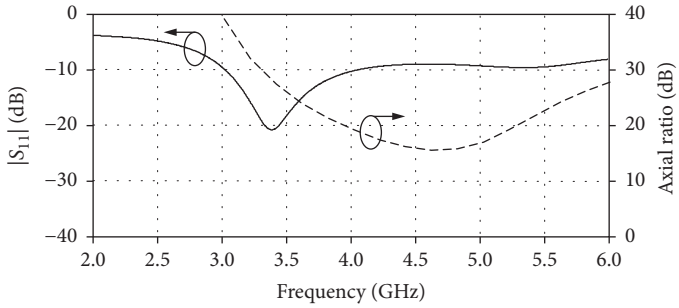

Figure 2: Simulated results of the truncated square patch antenna.

band with good isolation together. There is also the antenna [21] that used a stacked patch and U-slot to achieve dual-band circularly polarized characteristic. However, stacking many elements together leads to an increase in overall size of the antenna.

This experimental research thus proposes a dual-frequency (2.4 and 5.8 GHz) circularly polarized truncated square aperture patch antenna with slant stripline and L-shaped slot for WLAN applications. In the antenna evolution, a wide slot technique is utilized to realize the antenna minimization, the impedance bandwidth enhancement, and a bidirectional radiation pattern. The stripline rotation and L-shaped slot are incorporated to manipulate the antenna's surface current directions for circular polarization (CP). The design scheme aims to achieve the compact, cost-effective, circularly polarized dual-frequency operable antenna with satisfactory gains. A valuable improvement in axial ratio bandwidth is achieved with the proposed technique. The antenna is able to obtain the simulated and experimental lower-band axial ratios (AR) which were, respectively, 1.48 dB and 1.62 dB, with the corresponding bandwidths of 6.1% and 3.7%, while those of the upper band were 0.66 dB and 0.54 dB with the corresponding bandwidths of 8.4% and 6.0%.

The organization of the research paper is as follows: Section 1 is the introduction. Section 2 discusses the antenna structure and evolution with the simulation results of the proposed dual-band CP antenna. Section 3 compares the simulation and experimental results. The concluding remarks are provided in Section 4.

2. Antenna Structure and Evolution

Figure 1 illustrates the initial structure of the proposed antenna (antenna A). The antenna is designed on FR-4 substrate with a relative permittivity (ε_r) of 4.3 and loss tangent (δ) of 0.02. The antenna has a width (W) × length (L) × thickness (h) of 40 mm × 54 mm × 1.6 mm. On the front side of the antenna, there is a microstrip feed line with a width (w_f) × length (l_f) of 3.1 mm × 19 mm, which is a transmission line with an impedance of 50 Ω. A truncated square aperture slot is located on another side of the FR-4 substrate. The slot has a size of 23 mm × 23 mm with the chamfer width (w_c) of 3.5 mm and chamfer angle (α) of 45°. Performance of the antenna is shown in Figure 2. The current stage of antenna is single band and has linear polarization, which could be further improved.

In order to enhance the bandwidth of the proposed antenna, a parasitic patch is placed at the center of the truncated square aperture slot. This leads to the second design of the proposed antenna (antenna B) as shown in Figure 3. The parasitic patch was, respectively, 26.7 mm and 4 mm in width (w_t) and length (l_t) and clockwise-rotated with the angle of 45°. The introduction of slant strip creates a new impedance band along with the reduction in axial ratio near both resonance frequencies as illustrated in Figure 4.

The circularly polarized characteristic is adjusted by inserting an L-shaped slot at the bottom of the truncated square aperture. The final design of the proposed antenna (antenna C) is shown in Figure 5. The L-shaped slot has

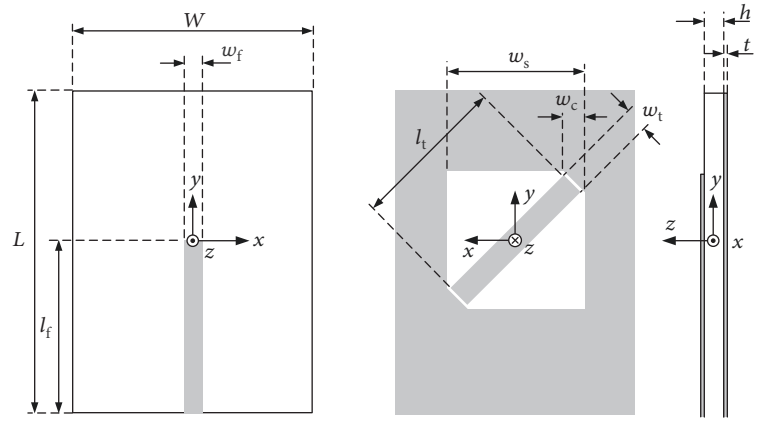

Figure 3: Structure of the truncated square patch antenna with slant strip (front view, rear view, and side view).

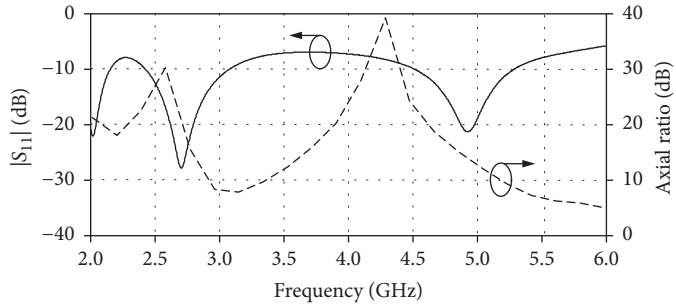

Figure 4: Simulated results of the truncated square patch antenna with slant strip.

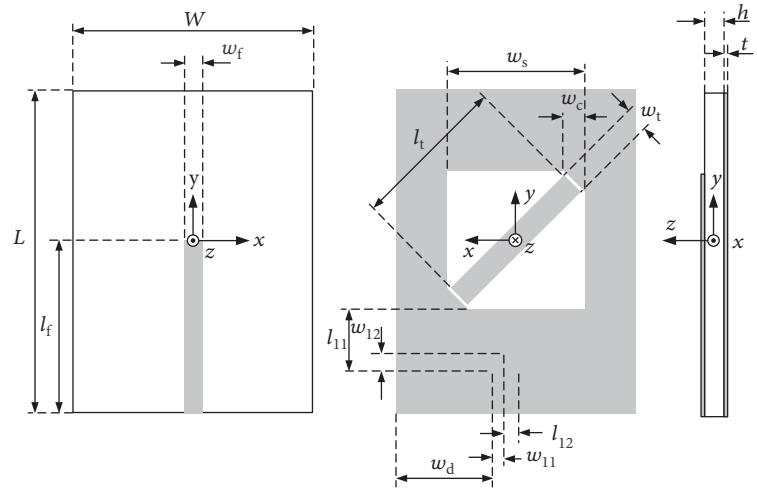

Figure 5: Structure of the truncated square aperture slot antenna with slant strip and L-shaped slot (front view, rear view, and side view).

a dimension of $w_{l1} = 2$ mm, $l_{l1} = 10.5$ mm, $w_{l2} = 3$ mm, $l_{l2} = 2.5$ mm, and $w_d = 16$ mm. This change in the structure results in the proposed antenna being dual-frequency circularly polarized as can be seen in Figure 6.

The variation in dimensions of the truncated square slot (w_s and w_c) leads to the shift in resonance band as shown in Figure 7. Figure 7(a) indicates that the square slot width (w_s) has a significant effect on $|S_{11}|$ of the proposed antenna. Therefore, the square slot width of $w_s = 23$ mm is chosen as it provides a good coverage over the interested bands. The size of truncated cuts affect mainly on axial ration of the antenna as can be seen in Figures 7(c) and 7(d). Hence, the truncated size of $w_c = 3.5$ mm is picked, because it gives lower axial ratio value during the interested bands.

Figure 8 illustrates an effect of the slant strip on the antenna performance. Both length and width of the slant strip (l_t and w_t) do not have any significant impact on the frequency coverage during the interested bands as shown in Figures 8(a) and 8(c). Thus, the length and width of $w_t = 3$ mm and $l_t = 26.7$ mm are selected, due to the fact that

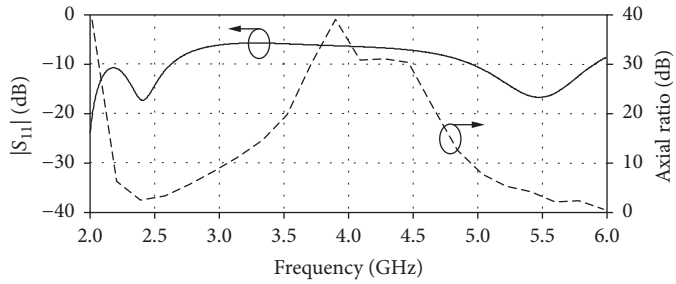

Figure 6: Simulated results of the truncated square patch antenna with slant strip and L-shaped slot.

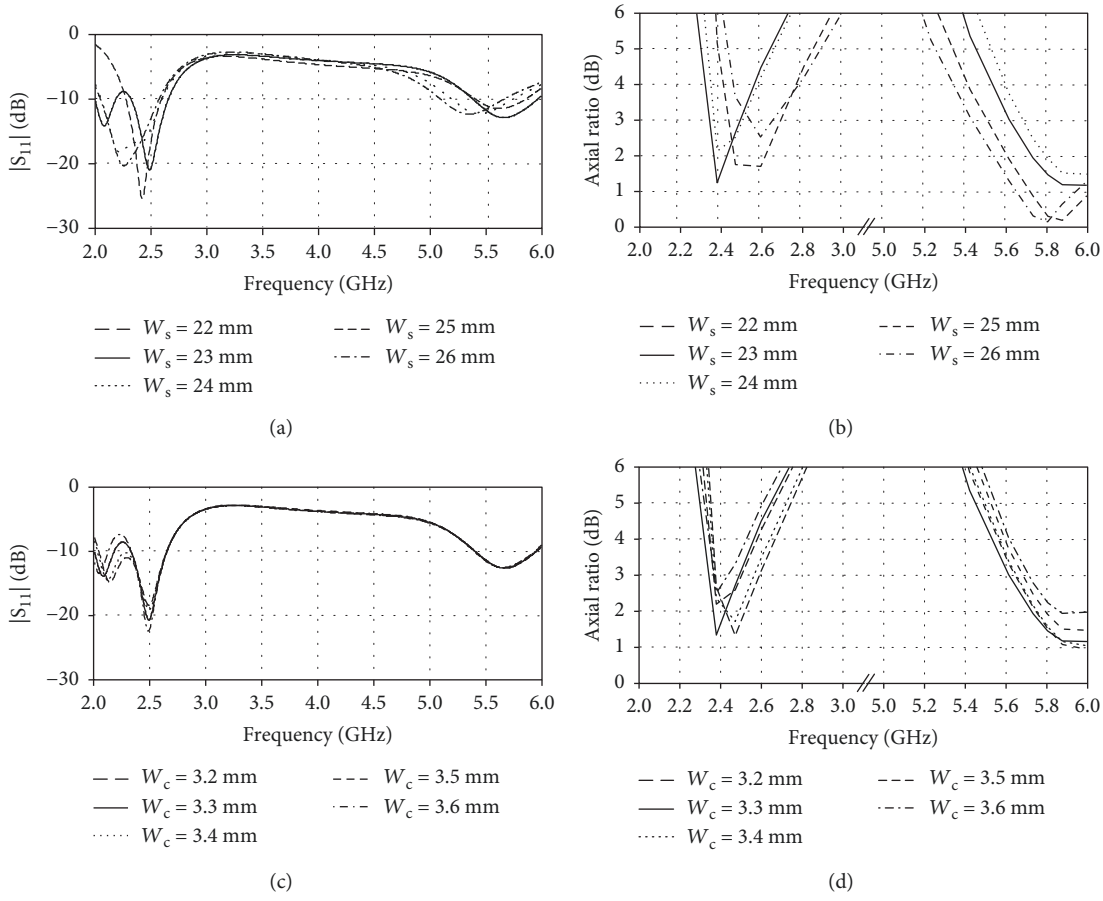

Figure 7: Simulated results of the proposed antenna: (a) $|S_{11}|$ when w_s is varied, (b) axial ratio when w_s is varied, (c) $|S_{11}|$ when w_c is varied, (d) and axial ratio when w_c is varied.

they provide the lowest axial ratio value at the interested frequency ranges, as illustrated in Figures 8(b) and 8(d).

Figure 9 presents the characteristic of the proposed antenna when the size of L-shaped slot is varied. Since the dimension of the L-shaped slot affects the outer border square slot's length, the change in resonance frequency can be expected as presented in Figures 9(a) and 9(c). However, L-shaped slot also introduces the change in current direction, which results in an ability to fine tune the polarization of the proposed antenna. Hence, the L-shaped slot with a sizing of $l_{l1} = 10.5$ mm and $l_{l2} = 3.0$ mm is selected as an optimized value for the lowest axial ratio possible on both interested frequency bands, as can be seen in Figures 9(b) and 9(d).

Figures 10(a) and 10(b), respectively, illustrate the left hand and right hand circular polarization radiation patterns of the lower and upper WLAN bands of each design of the proposed antenna (antenna A, antenna B, and antenna C). Antennas A, B, and C achieve the lower-band maximum radiated power at $\theta = -10^\circ$ (antenna front) and 170° (antenna rear); −5° and 175°; and 0° and 180°, respectively. Meanwhile, the upper-band maximum radiated power achieved by antennas A, B, and C were at $\theta = -15^\circ$ (antenna front) and 165° (antenna rear); −7° and 173°; and 0° and 180°,

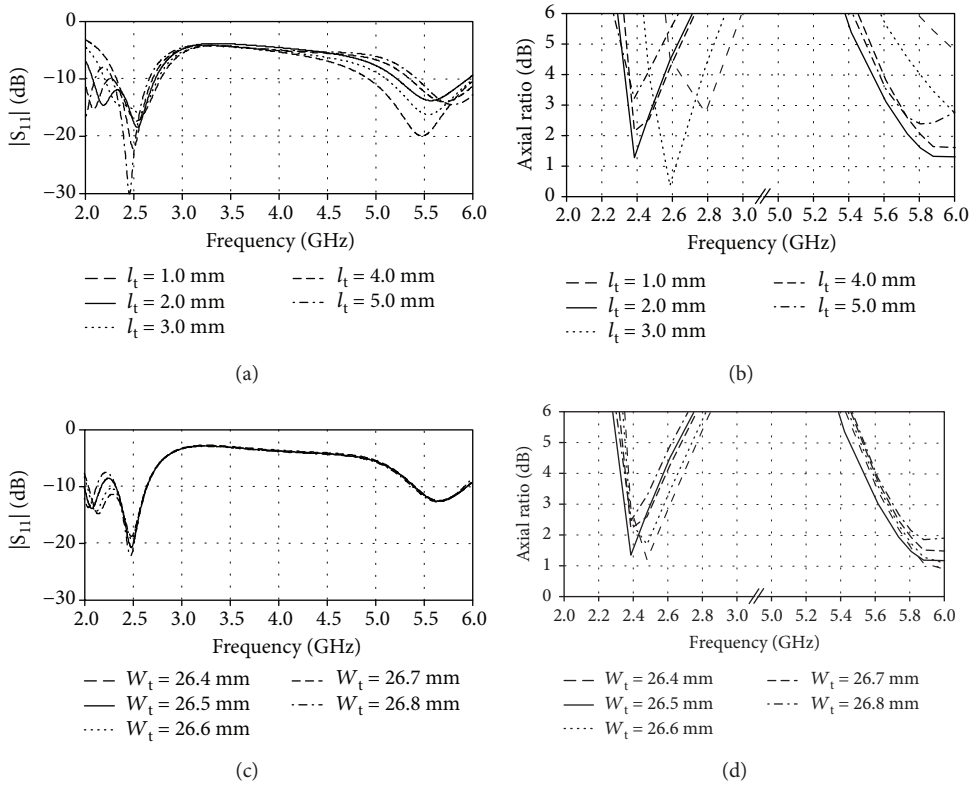

FIGURE 8: Simulated results of the proposed antenna: (a) $|S_{11}|$ when w_t is varied, (b) axial ratio when l_t is varied, (c) $|S_{11}|$ when w_t is varied, (d) and axial ratio when l_t is varied.

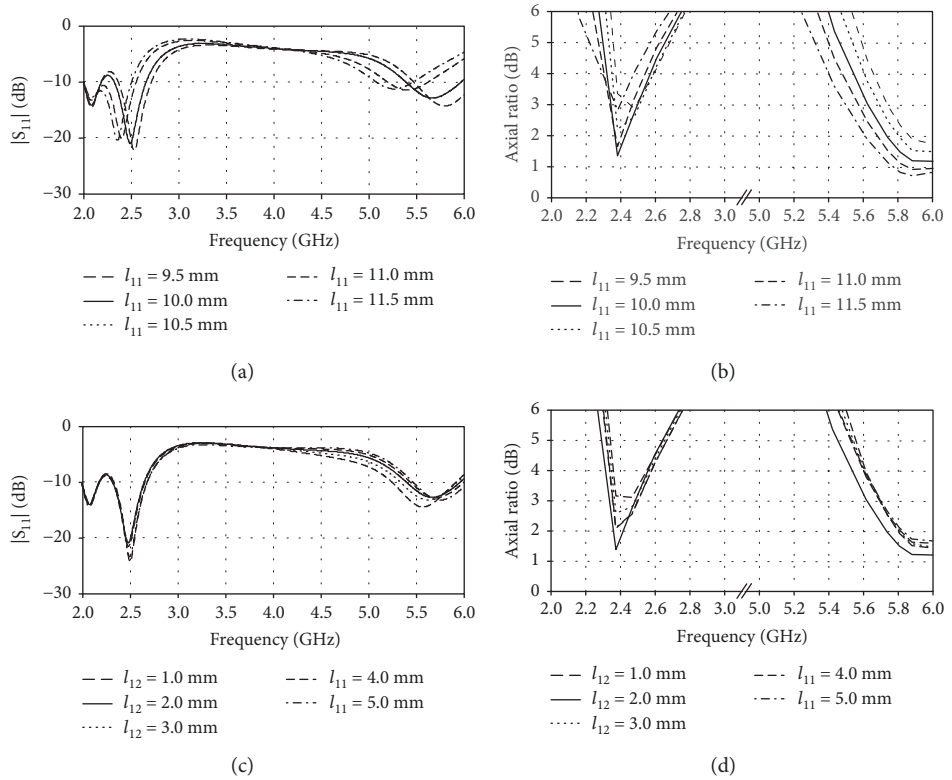

FIGURE 9: Simulated results of the proposed antenna: (a) $|S_{11}|$ when l_{l1} is varied, (b) axial ratio when l_{l1} is varied, (c) $|S_{11}|$ when l_{l2} is varied, (d) and axial ratio when l_{l2} is varied.

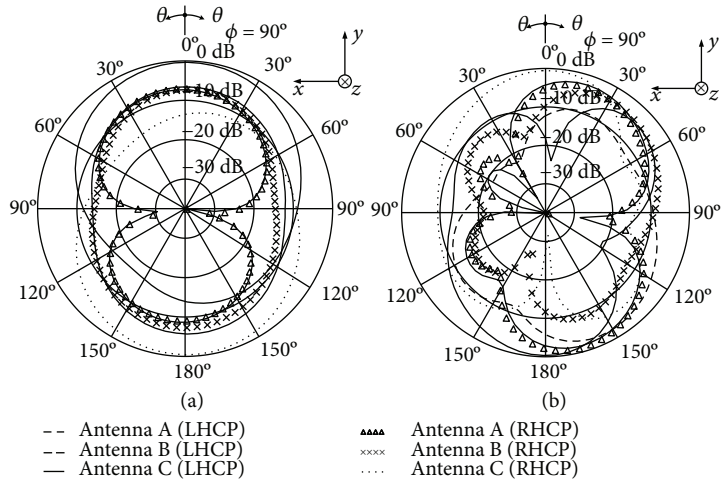

Figure 10: The left hand and right hand circular polarization radiation patterns of antenna A, antenna B, and antenna C: (a) 2.45 GHz; (b) 5.8 GHz.

Table 1: The optimal parameters of the proposed WLAN-enabled dual-frequency antenna.

Parameter	Description	Value (mm)	λ_0 2.45 GHz	λ_1 5.8 GHz
W	Antenna width	40	0.33	0.77
L	Antenna length	54	0.44	1.04
w_1	Feed line width	3.1	0.03	0.06
w_2	Rectangular truncated square aperture width	23	0.19	0.44
w_3	Chamfer width	23	0.19	0.44
w_4	Stripline width	4	0.03	0.08
w_5	L-shaped truncated aperture gap	1.5	0.01	0.03
w_6	L-shaped leg truncated aperture width	2	0.02	0.04
w_7	L-shaped foot truncated aperture width	3	0.02	0.06
l_1	Feed line length	29	0.24	0.56
l_2	Stripline length	4	0.03	0.08
l_3	L-shaped leg length	10.5	0.09	0.20
l_4	L-shaped foot length	3	0.02	0.06
h	Substrate thickness	1.6	0.01	0.03
t	Copper thickness	0.05	0.0004	0.001
α	Chamfer angle	45°	—	—
β	Strip angle	45°	—	—
ε_r	Relative permittivity	4.3	—	—

respectively. The realized maximum radiated power at $\theta = 0^\circ$ and 180° (i.e., ideal bidirectional radiation pattern) of antenna C was attributable to the foot of the L-shaped slot (w_7). Table 1 tabulates the optimal parameters of the proposed WLAN-enabled dual-frequency circularly polarized truncated square aperture patch antenna with slant stripline and L-shaped slot.

3. Simulation and Experimental Results

Simulations were carried out with the proposed WLAN-enabled antenna (antenna C), realized according to the

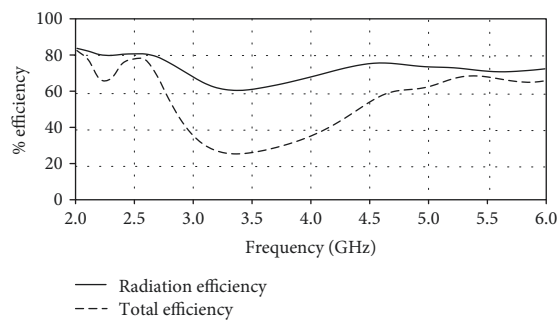

Figure 11: The simulated radiation and total efficiencies of the proposed WLAN-enabled dual-frequency antenna.

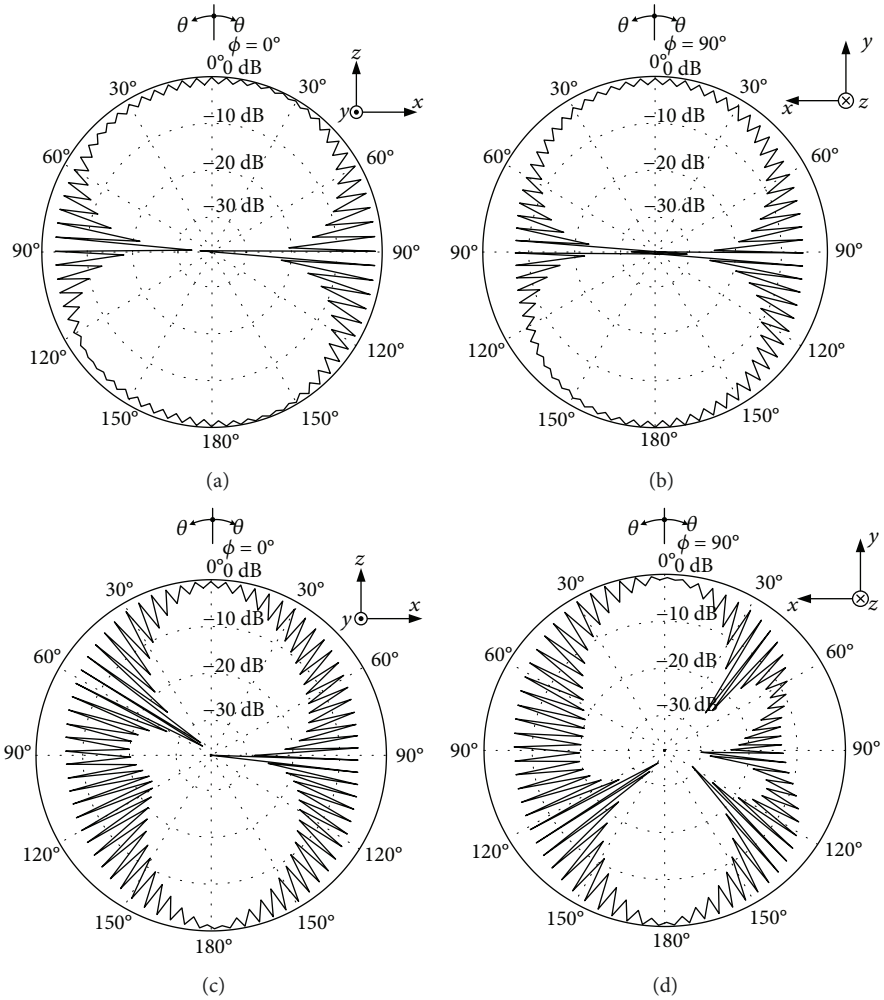

FIGURE 12: The simulated axial ratio radiation patterns: (a) 2.45 GHz at $\phi = 0^{\circ}$, (b) 2.45 GHz at $\phi = 90^{\circ}$, (c) 5.8 GHz at $\phi = 0^{\circ}$, (d) and 5.8 GHz at $\phi = 90^{\circ}$.

optimal antenna parameters (Table 1). Figure 11 illustrates the simulated radiation efficiency and total efficiency of the proposed dual-frequency antenna. The lower- and upper-band radiation and total efficiencies were 80% and 72%; and 75% and 68%, respectively.

The measured radiation patterns are performed in the receiving mode in anechoic chamber. The measurement setup uses an identical transmitting and receiving antennas separated by a distance R, which is satisfied the far-field criterion. Figures 12(a)–12(d), respectively, illustrate the simulated lower- and upper-band axial ratio radiation patterns at $\phi = 0^{\circ}$ and 90°. In the figure, at the operating angles ($\theta = 0^{\circ}$ and 180°), given the close proximity between the peak and trough of the axial ratio radiation pattern, the axial ratios (AR) were close to 0 ($\mathrm{AR} \leq 3$ dB). The lower-band beamwidths were between -43.5° and 43°; and -43° and 43.5° for the antenna front and rear, and the corresponding upper-band beamwidths were between -29.5° and 55°; and 33° and -51°.

Figures 13(a) and 13(b), respectively, illustrate the simulated lower- and upper-band current vector distributions of the proposed antenna (front view). The direction of the lower- and upper-band surface current was $t = 0$, $t = T/4$, $t = 3T/4$, and $t = T/2$, resulting in the circular polarization.

Figure 14 depicts the front and rear views of the antenna prototype fabricated as per the optimal antenna parameters. Figure 15 compares the simulated and experimental $|S_{11}|$ of the proposed antenna. The simulated and experimental lower-band $|S_{11}|$ were, respectively -14.81 dB and -13.92 dB, with the corresponding bandwidths ($|S_{11}| < -10$ dB) of 2.364–2.585 GHz (9.0%) and 2.0–2.5 GHz (20.4%). On the other hand, the simulated and experimental upper-band $|S_{11}|$ were -10.91 dB and -19.23 dB with the corresponding bandwidths ($|S_{11}| < -10$ dB) of 5.144–6.0 GHz (14.8%) and 5.09–6.0 GHz (15.68%).

The measured boresight gain based on Friis transmission formula can be achieved by the swept-frequency. Figure 16 illustrates the simulated and experimental gains of the proposed WLAN-enabled dual-frequency antenna. The simulated and experimental lower-band gains were 2.51 dBic and 2.98 dBic, and the corresponding upper-band gains were 3.51 dBic and 3.49 dBic.

Figure 17 illustrates the simulated and experimental axial ratios (AR) of the proposed antenna. The simulated

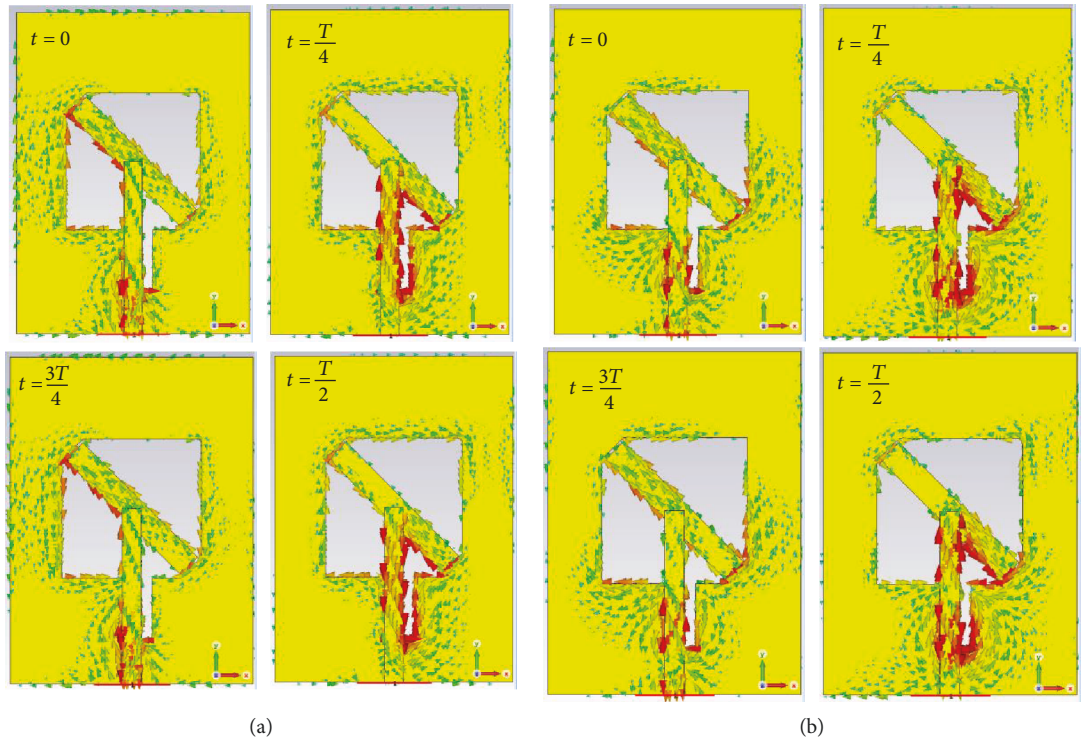

Figure 13: The current vector distributions of the proposed WLAN-enabled antenna (front view): (a) 2.45 GHz and (b) 5.80 GHz.

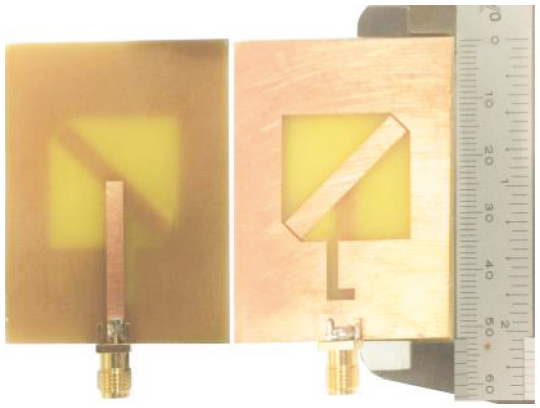

Figure 14: The front and rear view of the prototype of the proposed dual-frequency WLAN-enabled antenna.

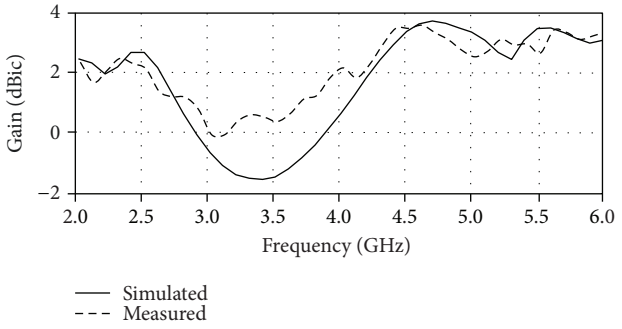

Figure 16: The simulated and experimental gains relative to frequency of the proposed antenna.

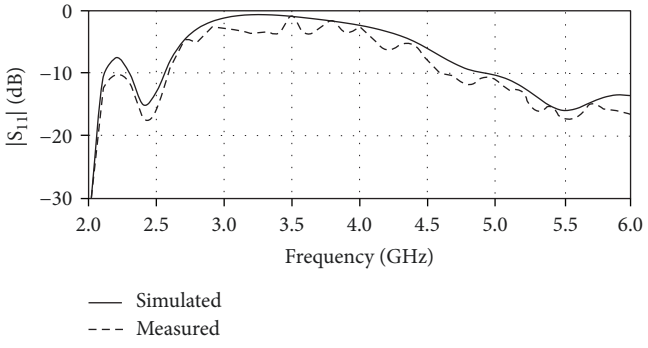

Figure 15: The simulated and experimental $|S_{11}|$ relative to frequency of the proposed antenna.

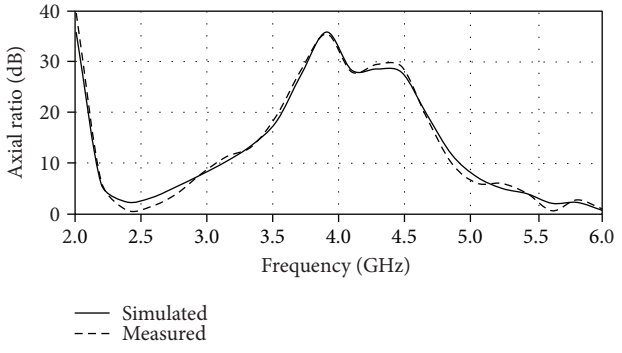

Figure 17: The simulated and experimental axial ratios relative to frequency of the proposed antenna.

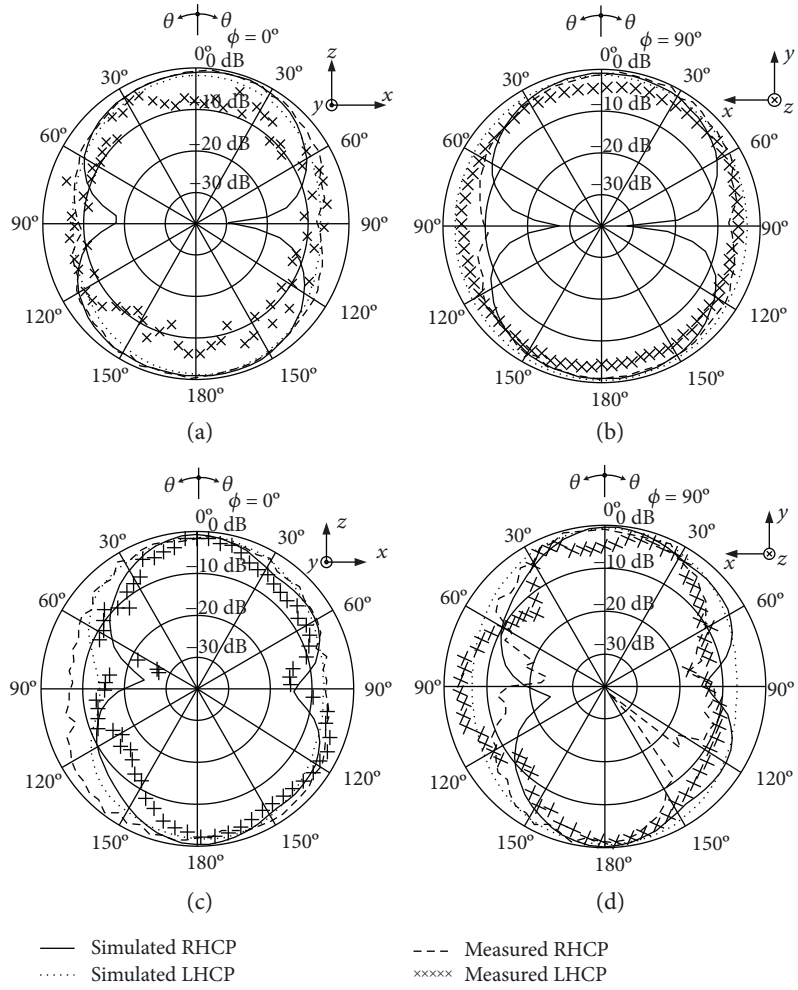

Figure 18: The simulated and experimental radiation patterns: (a) 2.45 GHz at $\phi = 0^{\circ}$, (b) 2.45 GHz at $\phi = 90^{\circ}$, (c) 5.8 GHz at $\phi = 0^{\circ}$, (d) and 5.8 GHz at $\phi = 90^{\circ}$.

and experimental lower-band AR were, respectively, 1.48 dB and 1.62 dB, with the corresponding bandwidths (AR ≤ 3 dB) of 2.38–2.53 GHz (6.1%) and 2.4–2.49 GHz (3.7%). On the other hand, the simulated and experimental upper-band AR were 0.66 dB and 0.54 dB, with the corresponding bandwidths (AR ≤ 3 dB) of 5.51–6.0 GHz (8.4%) and 5.58–5.93 GHz (6.0%).

Figures 18(a)–18(d), respectively, illustrate the simulated and experimental lower- and upper-band radiation patterns at $\phi = 0^{\circ}$ and 90°. In the figure, the simulated and experimental lower-band beamwidths at $\theta = 0^{\circ}$ and 180° were, respectively, from -43.5° to 43° and -43.5° to 43° (antenna front) and -43° to 43.5° and -41° to 42° (antenna rear). Meanwhile, the simulated and experimental upper-band beamwidths at $\theta = 0^{\circ}$ and 180° were from -29.5° to 55° and -27° to 50° (antenna front) and 33° to -51° and 26.5° to -51° (antenna rear), respectively.

Essentially, the simulated and experimental $|S_{11}|$, axial ratios, gains, and radiation patterns are in good agreement. Moreover, the proposed antenna exhibits the circular polarization and is operable in the dual-frequency WLAN bands (2.40–2.484 GHz and 5.725–5.875 GHz). The comparison characteristics of the proposed antenna with the existing works are summarized in Table 2. It can be seen that the proposed antenna provides the best axial ratio bandwidth on both operating frequencies.

4. Conclusion

This research has presented the WLAN-enabled dual-frequency circularly polarized truncated square aperture patch antenna with slant stripline and L-shaped slot. The antenna development involved three evolutionary stages where the simulations were performed using CST Microwave Studio for the optimal antenna parameters. The WLAN-enabled dual-frequency circularly polarized antenna was subsequently realized and simulated for $|S_{11}|$ (<−10 dB), the axial ratio (≤3 dB), gain, and radiation pattern. To validate, a prototype of the dual-frequency circularly polarized truncated square aperture patch antenna with slant stripline and L-shaped slot was fabricated and the experiments were carried out. The findings indicated the congruity between the simulated and experimental $|S_{11}|$, axial ratios, gains, and bidirectional radiation patterns. Specifically, the simulated and experimental $|S_{11}|$ for the lower band (2.40–2.484 GHz) were, respectively, −14.81 dB and −13.92 dB, with the

Table 2: The comparison of characteristics of the proposed antenna with the existing works.

Reference	Low band					High band					Dimension (mm^3)/substrate
	f_c (GHz)	$\|S_{11}\|$ BW (%)	AR BW (%)	Gain (dBic)	Global BW (%)	f_c (GHz)	$\|S_{11}\|$ BW (%)	AR BW (%)	Gain (dBic)	Global BW (%)	
Proposed	2.45	8.93	6.10	2.51	6.10	5.75	15.36	8.40	3.51	15.36	$40 \times 54 \times 1.6$/FR4
[8]	1.16	16.17	5.77	1.35	5.77	1.57	12.47	0.57	3.50	0.57	$84 \times 84 \times 21.5$/RO4003
[10]	1.63	2.93	1.10	4.00	1.10	2.88	2.42	1.04	1.50	1.04	$75 \times 75 \times 1.6$/FR4
[12]	2.47	8.03	6.06	2.93	6.06	3.50	6.86	5.71	6.26	5.71	$35 \times 35 \times 5.3$/R04003
[15]	2.44	15.83	2.86	5.59	2.86	5.67	3.45	2.64	3.00	2.64	$36 \times 36 \times 21$/Foam
[16]	1.21	4.18	0.83	1.35	0.83	1.46	3.39	0.68	3.50	0.68	$60 \times 60 \times 1.52$/FR4
[21]	3.43	2.86	2.04	6.20	2.04	5.84	15.64	3.27	6.50	3.27	$50 \times 50 \times 6.35$/Rogers 5880

corresponding bandwidths of 2.364–2.585 GHz (9.0%) and 2.0–2.5 GHz (20.4%). Meanwhile, the simulated and experimental upper-band (5.725–5.875 GHz) $|S_{11}|$ were −10.91 dB and −19.23 dB with the corresponding bandwidths of 5.144–6.0 GHz (14.8%) and 5.09–6.0 GHz (15.68%). The simulated and experimental lower-band axial ratios (AR) were, respectively, 1.48 dB and 1.62 dB, with the corresponding bandwidths of 2.38–2.53 GHz (6.1%) and 2.4–2.49 GHz (3.7%), while those of the upper band were 0.66 dB and 0.54 dB with the corresponding bandwidths of 5.51–6.0 GHz (8.4%) and 5.58–5.93 GHz (6.0%). For the antenna gain, the simulated and experimental lower-band gains were 2.51 dBic and 2.98 dBic; and those of the upper band were 3.51 dBic and 3.49 dBic. Moreover, both the simulated and experimental antennas achieved the lower- and upper-band maximum radiated power at $\theta = 0^\circ$ and 180°, indicating the bidirectional radiation pattern. In essence, the proposed WLAN-enabled dual-frequency antenna is applicable in both the vertically and horizontally elongated areas (e.g., in the tunnel, train carriage, and buildings), in addition to its compactness, lightweight, inexpensiveness, and ease of fabrication.

Data Availability

The data used to support the findings of this study are available from the corresponding author upon request.

Conflicts of Interest

The authors declare that there is no conflict of interests regarding the publication of this paper.

References

[1] C. A. Balanis, *Antenna Theory: Analysis and Design*, Wiley, New York, NY, USA, 3rd edition, 2005.

[2] J. Y. Jan and J. W. Su, "Bandwidth enhancement of a printed wide-slot antenna with a rotated slot," *IEEE Transactions on Antennas and Propagation*, vol. 53, no. 6, pp. 2111–2114, 2005.

[3] M. Samsuzzaman, M. T. Islam, J. S. Mandeep, and N. Misran, "Printed wide-slot antenna design with bandwidth and gain enhancement on low-cost substrate," *The Scientific World Journal*, vol. 2014, Article ID 804068, 10 pages, 2014.

[4] W.-L. Chen, G.-M. Wang, and C.-X. Zhang, "Bandwidth enhancement of a microstrip-line-fed printed wide-slot antenna with a fractal-shaped slot," *IEEE Transactions on Antennas and Propagation*, vol. 57, no. 7, pp. 2176–2179, 2009.

[5] F. Ferrero, C. Luxey, G. Jacquemod, and R. Staraj, "Dual-band circularly polarized microstrip antenna for satellite applications," *IEEE Antennas and Wireless Propagation Letters*, vol. 4, pp. 13–15, 2005.

[6] L. K. Hady, A. A. Kishk, and D. Kajfez, "Dual-band compact DRA with circular and monopole-like linear polarizations as a concept for GPS and WLAN applications," *IEEE Transactions on Antennas and Propagation*, vol. 57, no. 9, pp. 2591–2598, 2009.

[7] Y. J. Sung, "Circularly polarised square patch antenna with asymmetrical Y-shaped feed structure," *Electronics Letters*, vol. 46, no. 19, p. 1309, 2010.

[8] B. Li, Y. Ding, and Y.-Z. Yin, "A novel dual-band circularly polarized rectangular slot antenna," *International Journal of Antennas and Propagation*, vol. 2016, Article ID 9071610, 8 pages, 2016.

[9] F.-F. Fan, Z.-H. Yan, and W. Wang, "Wideband circularly polarized SIW antenna array that uses sequential rotation feeding," *International Journal of Antennas and Propagation*, vol. 2014, Article ID 534539, 8 pages, 2014.

[10] K. P. Yang and K. L. Wong, "Dual-band circularly-polarized square microstrip antenna," *IEEE Transactions on Antennas and Propagation*, vol. 49, no. 3, pp. 377–382, 2001.

[11] J. Y. Sze and C. C. Chang, "Circularly polarized square slot antenna with a pair of inverted-L grounded strips," *IEEE Antennas and Wireless Propagation Letters*, vol. 7, pp. 149–151, 2008.

[12] K. Agarwal and S. Dutta, "Miniaturized circularly polarized stacked patch antenna on reactive impedance surface for dual-band ISM and WiMAX applications," *International Journal of Antennas and Propagation*, vol. 2015, Article ID 938565, 10 pages, 2015.

[13] J. S. Row and S. W. Wu, "Circularly-polarized wide slot antenna loaded with a parasitic patch," *IEEE Transactions on Antennas and Propagation*, vol. 56, no. 9, pp. 2826–2832, 2008.

[14] X. Ye, M. He, P. Zhou, and H. Sun, "A compact single-feed circularly polarized microstrip antenna with symmetric and wide-beamwidth radiation pattern," *International Journal of Antennas and Propagation*, vol. 2013, Article ID 106516, 7 pages, 2013.

[15] Y. Ding and K. W. Leung, "Dual-band circularly polarized dual-slot antenna with a dielectric cover," *IEEE*

Transactions on Antennas and Propagation, vol. 57, no. 12, pp. 3757–3764, 2009.

[16] X. L. Bao and M. J. Ammann, "Dual-frequency circularly-polarized patch antenna with compact size and small frequency ratio," *IEEE Transactions on Antennas and Propagation*, vol. 55, no. 7, pp. 2104–2107, 2007.

[17] Nasimuddin, Z. N. Chen, and X. Qing, "Dual-band circularly polarized *S*-shaped slotted patch antenna with a small frequency-ratio," *IEEE Transactions on Antennas and Propagation*, vol. 58, no. 6, pp. 2112–2115, 2010.

[18] F. Yang and Y. Rahmat-Samii, "Switchable dual-band circularly polarised patch antenna with single feed," *Electronics Letters*, vol. 37, no. 16, p. 1002, 2001.

[19] G. Beigmohammadi, C. Ghobadi, J. Nourinia, and M. Ojaroudi, "Small square slot antenna with circular polarisation characteristics for WLAN/WiMAX applications," *Electronics Letters*, vol. 46, no. 10, pp. 672-673, 2010.

[20] G. Liu, L. Xu, and Y. Wang, "Modified dual-band stacked circularly polarized microstrip antenna," *International Journal of Antennas and Propagation*, vol. 2013, Article ID 382958, 5 pages, 2013.

[21] P. Nayeri, K. F. Lee, Z. Elsherbeni, and F. Yang, "Dual-band circularly polarized antennas using stacked patches with asymmetric U-slots," *IEEE Antennas and Wireless Propagation Letters*, vol. 10, pp. 492–495, 2011.